Manifestation of quantum rotor orbital excitations in Raman spectra of Jahn-Teller crystal $LaMnO_3$

2017 J. Phys.: Conf. Ser. 833 012005

(http://iopscience.iop.org/1742-6596/833/1/012005)

IOP Conf. Series: Journal of Physics: Conf. Series **833** (2017) 012005 doi:10.1088/1742-6596/833/1/012005

Manifestation of quantum rotor orbital excitations in Raman spectra of Jahn-Teller crystal $LaMnO_3$

N N Kovaleva[1,2], O E Kusmartseva[2], K I Kugel[3,4], F V Kusmartsev[2]

[1] Lebedev Institute of Physics, Russian Academy of Sciences, Moscow, Leninsky prosp. 53, 119991, Russia
[2] Department of Physics, Loughborough University, Loughborough, LE11 3TU, UK
[3] Institute for Theoretical and Applied Electrodynamics, Russian Academy of Sciences, Moscow, Izhorskaya street 13, 125412, Russia
[4] National Research University Higher School of Economics, Moscow, 109028, Russia

E-mail: nkovaleva@sci.lebedev.ru

Abstract. Materials, consisting of Jahn-Teller (JT) ions, such as cuprates and manganites, display many outstanding properties, including high temperature superconductivity and colossal magnetoresistance. There, the role of JT effect, although widely recognized, is still elusive. Here we show that these materials have vibronic excitations, related to local deformations rotating around JT ions in the dynamic limit, arising from linear electron-vibrational coupling in the "Mexican hat" potential profile. Their energy depends on total angular momentum, which is quantized, as in quantum rotors. We found them in the representative JT compound of orthorhombic manganites, $LaMnO_3$. Since the "Mexican hat" potential energy surface is double-valued, they show up near the ground and excited states of JT ions. Recently, by using spectroscopic ellipsometry technique, we showed that they appear in the excited state in the form of sidebands, accompanying the electron transition between the JT split orbitals at neighboring Mn^{3+} ions. Here, by using Raman scattering technique, we show that they also exist near the ground state. The found quantum rotor excitations may play an important role in many unusual properties observed in these materials.

1. Introduction

Orbital degeneracy, for example, the twofold degeneracy of e symmetry electronic orbitals of $Cu^{2+}(3d^9)$ or Mn^{3+} $(3d^4)$ ions in cubic symmetry, leads to peculiar behaviour when there is linear electron-lattice coupling. The linear electron-lattice coupling can be traced to the Jahn-Teller theorem [1], which states that a system, such as a complex in a solid or a molecule, which has a ground state possessing any degeneracy other than Kramers degeneracy, can achieve a lower energy by a distortion which removes the degeneracy. The undistorted geometry of $Cu^{2+}(3d^9)$ or Mn^{3+} $(3d^4)$ ions in sixfold coordination is octahedral, and the d orbitals split into a doublet (e) and a triplet (t_{2g}). In the undistorted cubic environment the ground state with the unpaired electron in the doublet is orbitally degenerate. The two degenerate $d(e)$ orbitals, $|\epsilon\rangle$ and $|\theta\rangle$, transform as x^2-y^2 and $2z^2-x^2-y^2$ under the octahedral group O_h, respectively. They are said to have e- or E-type symmetry. The octahedral complex may achieve lower energy by the three possible tetragonal distortions along the three distinct cubic axes, of which, only two, named as Q_2 and Q_3, are independent. They transform under the octahedral group O_h like the electronic wave functions $|\epsilon\rangle$ and $|\theta\rangle$, respectively. The symmetrized Q_2 and Q_3 displacements of

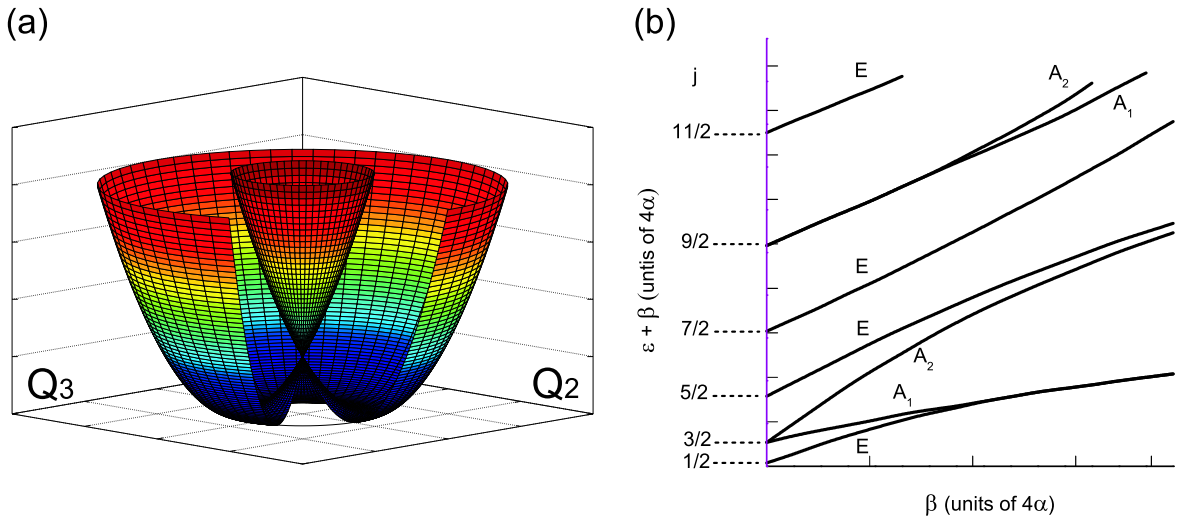

Figure 1. (a) Double-valued "Mexican hat" adiabatic potential energy surface for linear vibronic coupling (dynamic limit) in the normal coordinates Q_2 and Q_3. The "Mexican hat" perturbed by third-order (anharmonicity) terms has three discrete minima at the bottom of the through, separated by anharmonicity barriers (not shown). (b) Energies ε of the "Mexican hat" potential as functions of the barrier parameter β. The energy splitting parameter α is used in the quantization of discrete energy levels. Values of the angular momentum j=1/2, 3/2, 5/2, ... are given in the dynamic limit. Results after O'Brien [2].

the neighbours of transition-metal ions $Cu^{2+}(3d^9)$ or Mn^{3+} $(3d^4)$ in an octahedral environment correspond to the tetragonal normal modes of E symmetry.

The total (vibronic) energy of such JT complex is the sum of the JT energy and the elastic energy. It can be represented by the adiabatic potential-energy surface

$$V = \pm A\sqrt{Q_2^2 + Q_3^2} + \frac{1}{2}M\omega^2\left(Q_2^2 + Q_3^2\right), \tag{1}$$

where M is a mass of a corner atom, and ω is a circular vibrational frequency in the Q_2 or Q_3 normal modes (in the absence of JT effect). It is convenient to transform Eq. (1) to polar co-ordinates, $\rho \equiv \sqrt{Q_2^2 + Q_3^2}$ and $\phi \equiv \tan^{-1}\left(\frac{Q_2}{Q_3}\right)$

$$V = \pm A\rho + \frac{1}{2}M\omega^2\rho^2. \tag{2}$$

The adiabatic potential-energy surface represented by Eqs. (1) and (2) has some important features. First, it is double valued. The twofold degeneracy is lifted here, as for a given distortion we have two states, corresponding to the lower and upper sheets of the potential-energy surface. Second, the ground state energy is now lower by the JT energy, $E_{\mathrm{JT}} = -\frac{A^2}{2M\omega^2}$. And third, both potential-energy surfaces are independent of an angle ϕ, and the number of equivalent minimum-energy configurations is infinite. This means that the ground state energy is not uniquely defined, but occurs at any point of the circle with the radius $|\rho_0| = \frac{A}{M\omega^2}$ along the trough at the bottom of the lower potential-energy surface. This potential-energy surface for a doubly degenerate electronic state of e symmetry coupled to tetragonal E- symmetry vibrational modes has the so-called "Mexican hat" structure (see Fig. 1(a)). There are no barriers to prevent rotations in ϕ, which leads to the oscillations in the configuration of an octahedron without change in energy. This behaviour is known as the dynamic JT effect.

However, the infinite degeneracy of the ground state achieved for all values $\phi \equiv \tan^{-1}\left(\frac{Q_{20}}{Q_{30}}\right)$ in linear coupling may be removed if one takes into account higher-order coupling terms connecting the degenerate electronic states, which are of quadratic or higher order in the displacements Q_2 and Q_3. In particular, it was shown that the quadratic vibronic coupling essentially perturbs the ground state of the $e \otimes E$ Jahn-Teller systems [3, 4]. This will single out discrete values of ϕ, resulting in the appearance of three minima in the trough of the "Mexican hat". The specific values of the angles ϕ do depend on the details of the higher order terms. The minima on the low energy surface of the deformed "Mexican hat" are separated by potential barriers. Surprisingly, by *ab initio* calculations, it was shown that the effect of the third-order (cubic) terms to the barrier height between the minima is higher than, or of the same order of magnitude of the quadratic contributions [4].

The effect of small cubic perturbations on the lowest energy state of the system of the correct symmetry, $V_3(\phi) = A_3(\rho)\rho^3\cos(3\phi)$, was considered by O'Brien [2]. This perturbation for the lower potential-energy surface $V = -A\rho + \frac{1}{2}M\omega^2 + A_3\rho^3\cos(3\phi)$, will lead to the three discrete minima at $\phi = 0, \pm 120°$, if $A_3 < 0$, or $\pm 90°, 180°$, if $A_3 > 0$. And at a sufficiently low temperature, the system may become localised in one of them, associated with the tetragonal static lattice distortion. If the minima on the low energy surface of the deformed "Mexican hat" are separated by relatively low potential barriers (compared with temperature), tunneling between the three potential wells and rapid reorientation in the configuration of the octahedra can still occur. In this dynamical regime, the third-order (anharmonicity) terms act as a perturbation on the freely-rotating "Mexican hat". The influence of the barriers on the stability of the ground state was considered by O'Brien [2], who first investigated the quantum energy levels in this system. Their eigenvalues associated with the $\mathbf{A_1}$, $\mathbf{A_2}$, and $\mathbf{E}$ irreducible representations of the C_{3v} symmetry group were estimated. The results are presented in the diagram as a function of the potential barrier height β (see Fig. 1(b)). There is also the energy splitting parameter α used in the quantization of discrete energy levels [2]. As follows from the diagram, the $\mathbf{E}$ energy level is associated with the ground state with the quantum number of the angular momentum around the potential trough $j = \pm 1/2$. In the dynamic limit ($\beta = 0$), energies of the rotor excitations generate a sequence determined by the quadratic dependence on values of the angular momentum j, $\varepsilon_j = \alpha j^2$. These levels are associated with the dynamic limit of rotor excitations. Their energy levels shift with increasing the barrier height β in a static limit. Thus, for the two extreme limits of the barrier height β, we can have a dynamic fast-rotation limit for $\beta = 0$ and a static slow-rotation limit for $\beta \to \infty$.

Orthorhombic rare-earth manganites $R\mathrm{MnO_3}$ (R = La, Pr, Nd, Sm, Eu, Gd, Tb, Dy) are regarded to be model JT compounds, exhibiting cooperative JT effect [3, 5, 6, 7]. These systems are perovskites with the $\mathrm{Mn^{3+}}$ ions having the $t_{2g}^3 e_g^1$ electronic configuration. Among them, $\mathrm{LaMnO_3}$ crystal is famous as an insulating parent compound for doped manganites exhibiting colossal magnetoresistance effect. Its high-temperature phase is nearly cubic, and at the orbital ordering temperature $T_{\mathrm{OO}} \simeq 780$ K it undergoes a transition into the orthorhombic orbitally ordered *Pbnm* structure with an antiferrodistorsive ordering of $\mathrm{MnO_6}$ octahedra [8]. In our recent study of polarised Raman scattering in the untwinned $\mathrm{LaMnO_3}$ crystal, we discovered that the multi-order PDOS feature observed there up to the fourth order is the sidebands on the low-energy mode at 25 $\mathrm{cm^{-1}}$ [9]. This specifies that the low-energy mode at 25 $\mathrm{cm^{-1}}$ stems from the tunneling transition between the potential energy minima arising near the JT $\mathrm{Mn^{3+}}$ ion due to lattice anharmonicity. From the relation for the tunneling frequency, $\alpha = \frac{\hbar^2}{2M\rho_0^2}$, using for $\omega \simeq 500$ $\mathrm{cm^{-1}}$ and taking for the ligand mass M the mass of an oxygen atom, we estimated $E_{\mathrm{JT}} \simeq 0.325$ eV. In addition, in the dielectric function spectra of the untwinned $\mathrm{LaMnO_3}$ crystal we observed excitations, whose energy spectrum is described in terms of the total angular momentum eigenstates and is quantized as in quantum rotors found in JT centers [10]. They

appear clearly as narrow sidebands accompanying the e_g electron transition between the JT split orbitals at neighbouring Mn^{3+} ions. These results are presented together with new experimental evidence of photoluminescence found in $LaMnO_3$. This supports our interpretation, implying vibronic origin of the quantum rotor orbital excitations. The observed quantum rotor orbital excitations can be related to the upper sheet of the "Mexican hat" adiabatic potential-energy surface [10]. The obtained experimental evidence suggests that $LaMnO_3$ exhibits behaviour peculiar of the dynamic JT regime, where tunneling and rapid reorientation in the octahedral configuration can still occur. That is, $LaMnO_3$ can be considered as being effectively in the regime of the O'Brien's diagram (see Fig. 1(b)) [2], where the lattice anharmonicity acts as a perturbation only.

In this paper, we present the results of the polarised first- and higher-order Raman scattering in the untwinned $LaMnO_3$ crystal, measured under different power of laser excitation. Apart from the anomalously strong, periodically repeated up to the fourth order, PDOS feature [9], we were able to identify additional weak features under high laser excitation power, which can be associated with the quantum rotor orbital excitations. The found behavior can be related to the lower sheet of the "Mexican hat" adiabatic potential-energy surface, specifying the ground state properties. These results are in agreement with our previous optical study, indicating the dynamic behavior of the JT effect in $LaMnO_3$ in the regime of the O'Brien's diagram (see Fig. 1(b)) [2].

2. Experimental approach

$LaMnO_3$ single crystals were grown using the crucible-free floating-zone method in a mirror furnace, equipped with an arc lamp [11]. The as-grown $LaMnO_3$ crystals are single phased. However, they exhibit heavily twinned domain patterns below the orbital ordering temperature $T_{OO} \simeq 780$ K, in the orthorhombic *Pbnm* structure. The particular pattern and the size of the domains depend on local temperature gradients and mechanical stresses, experienced during the growth stage. We were able to get rid of the twins from an essential part of the sample volume following the procedure, described in detail in our earlier study [12]. It was detected by single-crystal X-ray diffraction that the percentage of detwinning at some areas was as high as 95 % and over the entire surface it was at least 80 %. The orthorhombic [010] direction was identified as perpendicular to the crystal surface. The sample was also characterised by SQUID magnetometry measurements. We determined the antiferromagnetic transition temperature T_N at 139.6 K, which is typical for nearly oxygen-stoichiometric $LaMnO_3$ crystals.

The sample surface was polished to optical grade. Raman scattering spectra were acquired using a Raman-microscope spectrometer LabRAM HR (Horiba Jobin Yvon), equipped with a grating monochromator and a liquid-nitrogen cooled CCD detector. The LabRAM HR spectrometer has high spectral resolution (0.3 cm^{-1}/pixel at 633 nm), large spectral range of Raman shift from 100 to 6000 cm^{-1} and unique edge filter technology. HeNe laser operating at the wavelength 632.8 nm (1.96 eV), with appropriate filters, was used for excitation under different irradiation power. The $LaMnO_3$ crystal sample was mounted on a cold finger of the micro-cryostat, cooled with liquid nitrogen. We used the near-normal back-scattering geometry with an adjustable confocal pinhole. The propagation direction of the incident and scattered light was parallel to the [010] orthorhombic axis (in *Pbnm* symmetry notations) of the untwinned $LaMnO_3$ crystal. The Raman scattering spectra were recorded in the distinctive principle polarisations, using generic linear polarisation of the laser radiation while rotating the sample in the xz plane.

3. Experimental results

A factor-group analysis of the orthorhombic crystal structure of $LaMnO_3$ (*Pbnm*, D_{2h}^{16}) with 4 f.u./unit cell gives 24 Raman-active phonon modes, namely $7A_g$, $7B_{1g}$, $5B_{2g}$, and $5B_{3g}$ symmetry

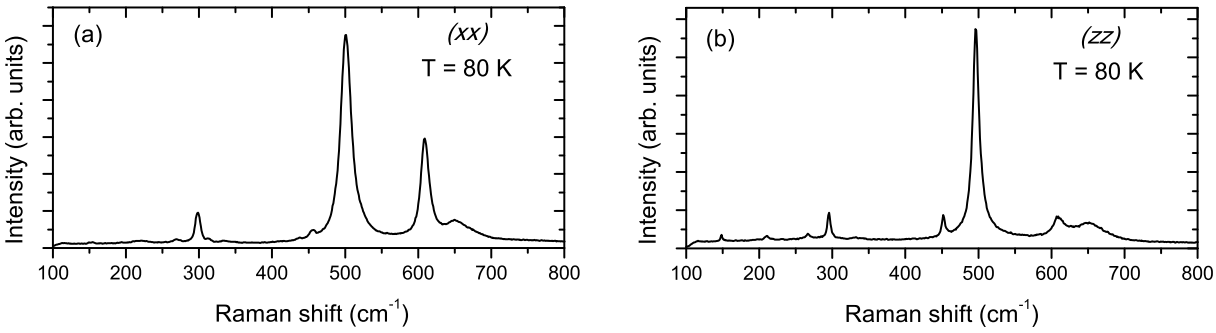

Figure 2. The low-temperature micro-Raman spectra ($T \simeq 80$ K), measured on the oriented xz surface of the untwinned $LaMnO_3$ crystal, with the incident laser light polarised along (a) the x axis and (b) the z axis (in $Pbnm$ symmetry notations). The HeNe laser operating at the wavelength 632.8 nm (1.96 eV) was used for excitation at low-level laser irradiation power (10%).

modes. The Raman scattering tensor determines the selection rule for Raman scattering. The normal modes of distinct symmetry could be observed under irradiation with a polarised light at a given scattering geometry. Accordingly, on the oriented crystal surface, the A_g symmetry phonons can be registered in the parallel (xx), (yy), and (zz) polarisations of the incident and scattered light, whereas the B_{1g}, B_{2g}, and B_{3g} phonons contribute in the crossed (xz, zx), (yz, zy), and (xy, yx) polarisations, respectively. All details on the different symmetry normal modes probed by the Raman scattering on the oriented xz surface of the untwinned $LaMnO_3$ crystal are given in our previous study [9]. As a result, we were able to identify the A_g symmetry modes at 148, 210, 267, 295, 452, and 495 cm^{-1} and the B_{1g} symmetry modes at 197, 313, 436, and 606 cm^{-1}. Figures 2(a) and (b) illustrate the low-temperature (80 K) micro-Raman spectra measured on the untwinned $LaMnO_3$ crystal for the two selected polarisations of the incident HeNe laser irradiation (at 10% laser irradiation power), along the main x and z crystallographic directions, respectively. Here, the pronounced high-frequency modes A_g (495 cm^{-1}) and B_{1g} (606 cm^{-1}) are assigned to the in-plane vibrations, due to the JT in-phase anti-symmetric and symmetric stretching of the corner-shared oxygen octahedra in $LaMnO_3$, respectively [13, 14, 15]. One may notice that the highest-frequency B_{1g} (606 cm^{-1}) mode is quite notably pronounced in the (xx) polarisation, whereas it is almost entirely suppressed in the (zz) polarisation. We would like to note that our Raman phonon spectra are in agreement with those of an earlier Raman study of an untwinned $LaMnO_3$ single crystal by Saitoh *et al.* [16], signifying the similar crystal quality. In our previous detailed temperature Raman study of the untwinned $LaMnO_3$ crystal [9], we find that the temperature coefficient of the full width at half maximum (FWHM) of the anti-symmetric JT A_g mode is about 0.07 ± 0.01 cm^{-1}/K, whereas for the symmetric JT B_{1g} mode it is about 0.04 ± 0.01 cm^{-1}/K.

In the one-phonon range of Raman scattering at higher frequencies an additional broad peak disposed at around 650 cm^{-1} is available (see Figs. 2(a) and (b)). It cannot be assigned to a normal symmetry mode in $LaMnO_3$ crystal structure. The excitation is also weakly infrared-active due to the parity-breaking effect. Moreover, the excitation demonstrates its general nature in all isovalent Mn^{3+} rare-earth $RMnO_3$ (R=La, Pr, Nd, Sm, Eu, Gd, Tb, Dy, Ho,Y) oxides, where it is present in the Raman spectra around the same frequency [17, 18]. As follows from our previous Raman scattering study, the excitation at 650 cm^{-1} is not a single mode; it is composed of $A_g + B_{1g}$ symmetry modes. Iliev *et al.* associates the Raman feature at 650 cm^{-1} with the maximum in the phonon density-of-states (PDOS) of oxygen vibrations, accordingly to polarisation properties and predictions, based on lattice-dynamics calculations [18, 19]. An

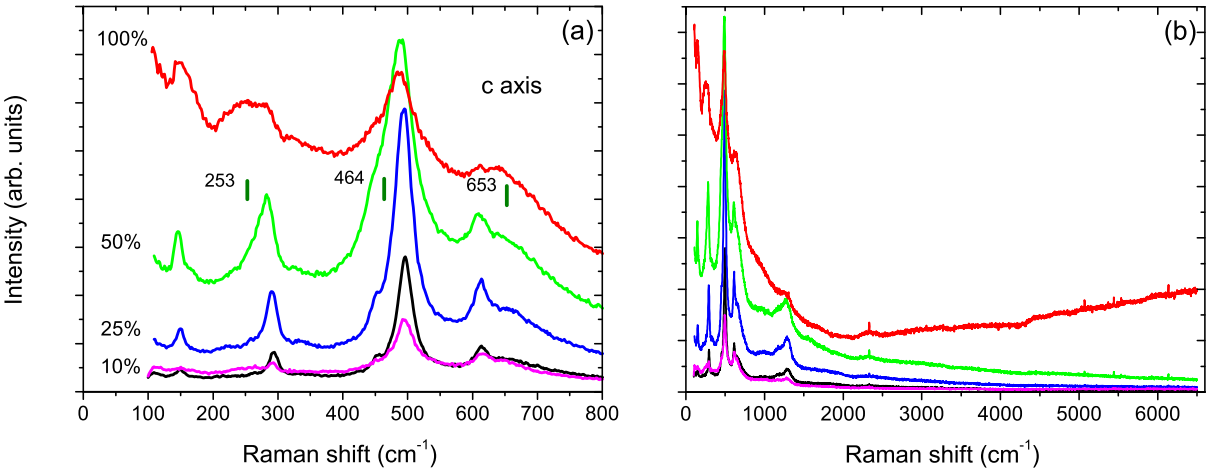

Figure 3. Dependence of the Raman scattering spectra measured at 300 K in parallel (zz) polarisations on the oriented xz surface of the untwinned $LaMnO_3$ crystal on the laser excitation power (a) in the one-phonon spectral range and (b) in the extended spectral range up to 6000 cm^{-1}. The local actual temperatures under the different laser excitation power, estimated from the width of the A_g phonon at 500 cm^{-1}: 10% (black curve) $\sim$ 300 K, 25% $\sim$ 400 K, 50% $\sim$ 600 K, 100% $\sim$ 700 K. The Raman scattering measurements repeated at 10% laser power (magenta curve) after finishing the cycle.

extended structure, represented by the three broad features, is developed in the second-order Raman scattering (see, for example, Fig. 4(b)). It demonstrates strong polarisation dependence, so that only one broad feature of A_g symmetry is visibly pronounced in the z-polarised spectra (see, for example, Fig. 3(b)). It was shown in our previous detailed study of the Raman scattering in $LaMnO_3$ [9] that in the multi-phonon spectral range the PDOS multiple excitations appear with a period of about 630 cm^{-1} up to the fourth order, shifted by about 25 cm^{-1} from the central laser line.

Figures 3(a) and (b) show dependence of the Raman scattering spectra on the laser excitation power, measured at 300 K in parallel (zz) polarisations on the oriented xz surface of the untwinned $LaMnO_3$ crystal, in the one-phonon spectral range and in the extended spectral range up to 6000 cm^{-1}. Using the linear temperature coefficient of the FWHM of the A_g mode at 500 cm^{-1}, 0.07 $\pm$ 0.01 cm^{-1}/K, obtained from our previous study [9], the local actual temperatures due to the sample heating under the laser irradiation with different power were estimated. We estimated that the sample heating is negligible under the laser irradiation with the laser power 10%. The obtained Raman scattering is consistent with the data shown in Fig. 2(b). Though, the overheating effect is appreciable under the laser irradiation with the laser power 100%, where the local actual temperature in the laser spot is estimated to be $\sim$700 K. However, the Raman scattering measurements repeated at 10% laser power after finishing the cycle indicate that there were no irreversible changes during the Raman measurements of the $LaMnO_3$ crystal under the used high-level power of the laser irradiation. One can follow the effect of broadening of the A_g mode at 500 cm^{-1} with increasing temperature from about 300 K under the laser irradiation with the laser power 10%, 25%, and 50% (see Fig. 3(a)). Here, in the extended spectral range, the PDOS feature shows up to the third order on the decreasing scattering background (see Fig. 3(b)). However, one can notice that additional broad features appear here under the 100% laser power. We fitted the obtained Raman spectra with a set of Lorentzians and determined that the additional features appear at 253, 464, and 653 cm^{-1}. At the same time, in the extended spectral range, the PDOS feature becomes almost suppressed

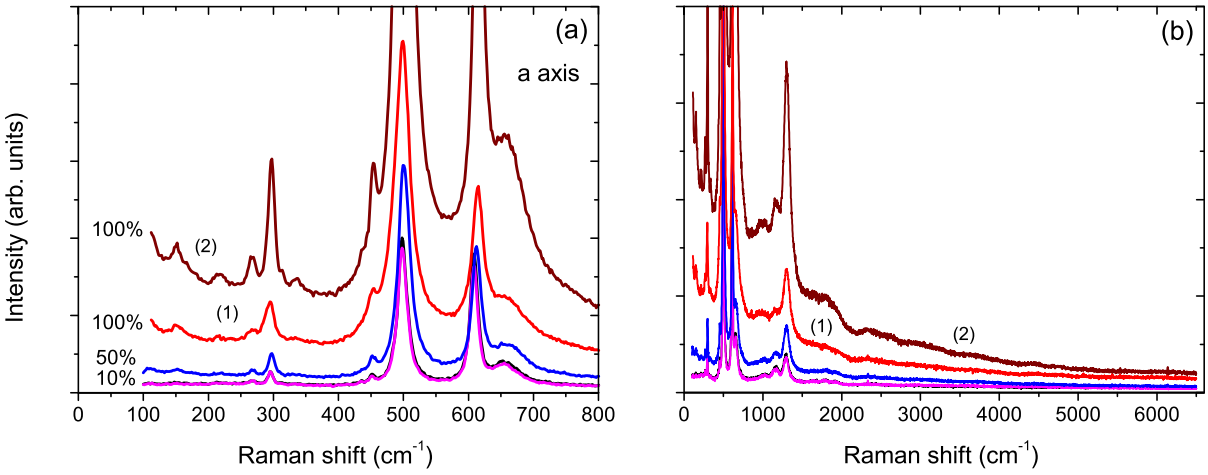

Figure 4. Dependence of the Raman scattering spectra measured at 80 K in parallel (xx) polarisations on the oriented xz surface of the untwinned $LaMnO_3$ crystal on the laser excitation power (a) in the one-phonon spectral range and (b) in the extended spectral range up to 6000 cm^{-1}. The local actual temperatures under the different laser excitation power, estimated from the width of the A_g phonon at 500 cm^{-1}: 10% (black curve) $\sim$ 80 K, 50% $\sim$ 180 K, 100% (1) and (2) $\sim$ 250 K. The Raman scattering measurements repeated at 10% laser power (magenta curve) after finishing the cycle.

by temperature. However, interestingly, a broad Raman scattering shows up on the increasing background above 2000 cm^{-1}, with some discernible superstructure in it (see Fig. 3(b)). The observed behavior is close to the orbital ordering temperature $T_{OO} \simeq 780$ K into the pseudo-cubic high-temperature phase [8]. Therefore, it can be associated with the fingerprints of the dynamic JT effect in $LaMnO_3$, where the energetic barriers in the "Mexican hat" potential profile become thermally accessible.

Figures 4(a) and (b) show dependence of the Raman scattering spectra on the laser excitation power, measured at 80 K in parallel (xx) polarisations on the oriented xz surface of the untwinned $LaMnO_3$ crystal in the one-phonon spectral range and in the extended spectral range up to 6000 cm^{-1}. The local actual temperatures under the different laser excitation power were estimated from the FWHM temperature dependence of the A_g phonon at 500 cm^{-1}. Similarly, we estimated that the sample heating is negligible under the laser irradiation with the laser power 10%, where the obtained Raman scattering results are consistent with the results shown in Fig. 2(a). However, the overheating effect is appreciable under the laser irradiation with the laser power 100%, where the local actual temperature in the laser spot is estimated to be $\sim$ 250 K. The Raman scattering measurements repeated at 10% laser power after finishing the cycle indicate no irreversible changes during the Raman measurements of the $LaMnO_3$ crystal under the used 100% power of the laser irradiation. Here, one can follow the effect of broadening of the A_g mode at 500 cm^{-1} with increasing temperature from about 80 K to about 250 K under the laser irradiation with the laser power 10%, 50%, and 100% (see Fig. 4(a)). In the extended spectral range, the PDOS feature is relatively more pronounced than in the corresponding z-polarised Raman spectra and shows up to the third order on the decreasing scattering background (see Fig. 4(b)).

Figures 5(a) and (b) demonstrate the Raman scattering spectra measured under the high laser irradiation power (100%) at different temperatures in parallel (xx) polarisations on the oriented xz surface of the untwinned $LaMnO_3$ crystal in the one-phonon spectral range and in the extended spectral range up to 6000 cm^{-1}, respectively. Due to strong overheating effect

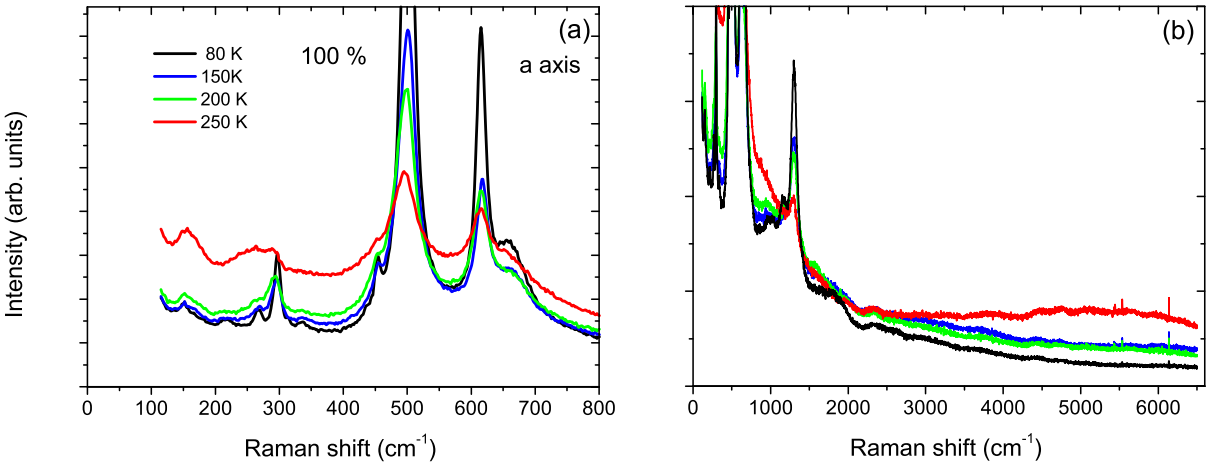

Figure 5. The Raman scattering spectra measured under the high laser excitation power (100%) at different temperatures in parallel (xx) polarisations on the oriented xz surface of the untwinned $LaMnO_3$ crystal (a) in the one-phonon spectral range and (b) in the extended spectral range up to 6000 cm^{-1}. The local temperatures in the laser spot, estimated from the FWHM of the A_g phonon mode at 500 cm^{-1}: $\sim$250 K for the measurements at 80 K, $\sim$370 K for the measurements at 150 K, $\sim$450 K for the measurements at 200 K, and $\sim$600 K for the measurements at 250 K.

under the high laser irradiation power, the local temperatures in the laser spot are different from the referred temperatures. These temperatures, estimated from the FWHM of the A_g phonon mode at 500 cm^{-1} are: $\sim$250 K for the measurements at 80 K, $\sim$370 K for the measurements at 150 K, $\sim$450 K for the measurements at 200 K, and $\sim$600 K for the measurements at 250 K. One can notice changes in the one-phonon range under the 100% laser power for the measurements at 250 K, similar to those observed in the z-polarized spectra under the 100% laser power in Fig. 3(a). At the same time, a broad Raman scattering shows up on the increasing background above 2000 cm^{-1}, with some discernible superstructure in it (see Fig. 5(b)). We guess that the observed behavior, close to orbital ordering temperature $T_{OO} \simeq 780$ K, can be associated with the fingerprints of the dynamic JT effect in $LaMnO_3$, where the energetic barriers in the "Mexican hat" potential profile become thermally accessible.

In Figs. 6(a) and (b) the Raman scattering spectra measured under the high laser irradiation power (100%) in parallel (xx) and (zz) polarisations on the oriented xz surface of the untwinned $LaMnO_3$ crystal in the spectral range up to 1000 cm^{-1} and in the extended spectral range from 1000 cm^{-1} to 6000 cm^{-1} are displayed. These Raman spectra correspond to the data shown in Figs. 3(a) and (b) and Figs. 5(a) and (b). Here, the local actual temperatures, estimated from the width of the A_g phonon at 500 cm^{-1} are relatively close to orbital ordering temperature $T_{OO} \simeq 780$ K: $\sim$600 K for the measurements at 250 K, $\sim$700 K for the measurements at 300 K. The observed behaviour in the one-phonon range and in the extended spectral range can be associated with the fingerprints of the dynamic JT effect in $LaMnO_3$ crystal. One can notice that similar changes are observed in parallel (xx) and (zz) polarisations on the oriented xz surface of the untwinned $LaMnO_3$ crystal, in the one-phonon spectral range and in the extended spectral range. The fine structure in Fig. 6(b) is represented by a set of the narrow lines, which are reproducible in both polarisations.

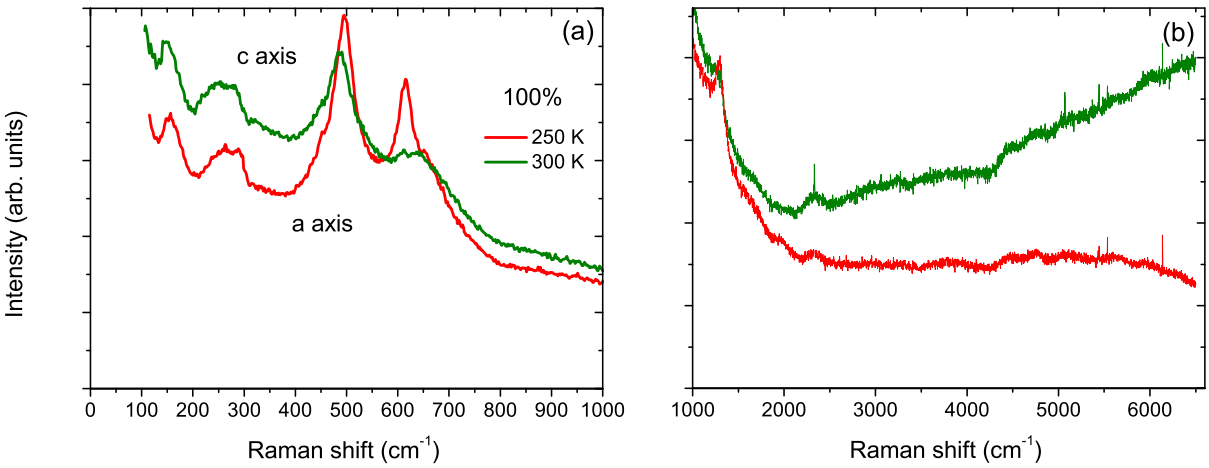

Figure 6. The Raman scattering spectra measured under high laser excitation power (100%) in parallel (xx) and (zz) polarisations on the oriented xz surface of the untwinned $LaMnO_3$ crystal in (a) the spectral range up to 1000 cm^{-1} and (b) the extended spectral range from 1000 cm^{-1} to 6000 cm^{-1}. The local actual temperatures, estimated from the width of the A_g phonon at 500 cm^{-1}: $\sim$600 K for the measurements at 250 K, $\sim$700 K for the measurements at 300 K.

4. Discussion and conclusions

We consider that the narrow lines appearing in the high-energy Raman scattering spectra close to the orbital ordering temperature, $T_{OO} \simeq 780$ K, are related to quantum rotor orbital excitations in a "Mexican hat" potential profile (see Fig. 1(a)). The quantum rotor orbital excitations are genuine electronic-vibrational (vibronic) excitations. Their eigenvalues, associated with the $\mathbf{A}_1$, $\mathbf{A}_2$, and $\mathbf{E}$ irreducible representations of the C_{3v} symmetry group, were earlier estimated by O'Brien and represented in the diagram as a function of the potential barrier height β (see Fig. 1(b)) [2]. As follows from the diagram, the $\mathbf{E}$ energy level is associated with the ground state with the quantum number of the angular momentum around the potential trough $j = \pm 1/2$. There is also the energy splitting parameter α used in the quantization of discrete energy levels [2]. In the dynamic limit ($\beta = 0$), energies of the rotor excitations generate a sequence determined by the quadratic dependence on values of the angular momentum j, $\varepsilon = \alpha j^2$. The $\mathbf{E}$ symmetry states are characterised by the angular momentum quantum numbers $j = 1/2, -5/2, 7/2, -11, 2, 13/2, \ldots$ and $j = -1/2, 5/2, -7/2, 11/2, -13/2, \ldots$. And the $\mathbf{A}_1$ and $\mathbf{A}_2$ symmetry states are characterised by the angular momentum quantum numbers $j = \pm 3/2, \pm 9/2, \pm 15/2, \pm 21/2, \pm 27/2, \ldots$. The tunneling splitting α is estimated at 25 cm^{-1} from our recent study of the anomalous multi-order Raman scattering in $LaMnO_3$ [9]. Here, using $\alpha = 25$ cm^{-1}, we evaluated the quantum rotor energies, obeying the square law $\varepsilon = \alpha j^2$. The estimated energies of the $\mathbf{A}_1$, $\mathbf{A}_2$, and $\mathbf{E}$ symmetry states, corresponding to modulus of the angular momentum quantum numbers j, are pointed on the top scale of Figs. 7(a)–(c). Figures 7(a)–(c) show the Raman scattering spectra measured at 300 K in parallel (zz) polarisations on the oriented xz surface of the untwinned $LaMnO_3$ crystal on the laser excitation power (also shown in Figs. 3(a) and (b)). The local actual temperature under 100% laser irradiation power, estimated from the width of the A_g phonon at 500 cm^{-1}, is of $\sim$700 K, rather close to the orbital ordering temperature $T_{OO} \simeq 780$ K. Here, the additional features pop up in the one-phonon spectral range at 253, 464, and 653 cm^{-1} and in the extended spectral range above 2000 cm^{-1}. The observed behaviour can be associated with the fingerprints of the dynamic JT effect in $LaMnO_3$ crystal. We predict that the features evident at high energies at $\sim$1960 cm^{-1} (0.243 eV), $\sim$2300 cm^{-1} (0.285 eV), $\sim$3260 cm^{-1} (0.404 eV), and $\sim$4460 cm^{-1} (0.553 eV) could be

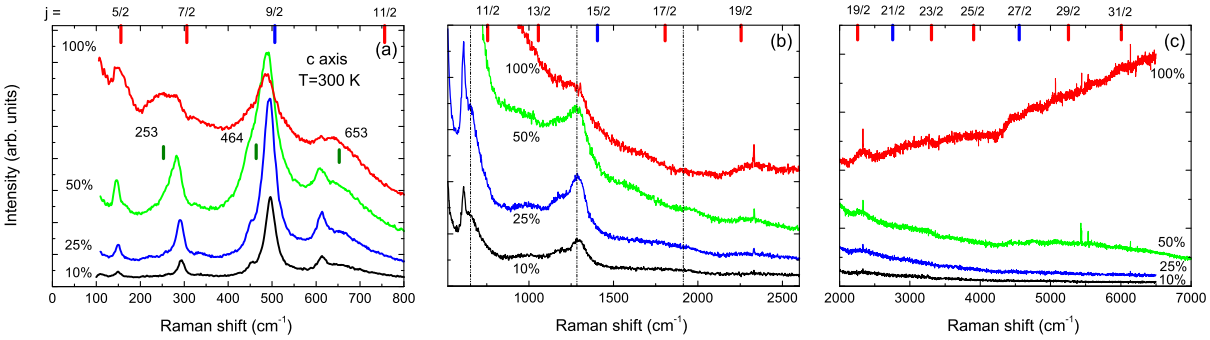

Figure 7. The Raman scattering spectra measured at 300 K in parallel (zz) polarisations on the oriented xz surface of the untwinned $LaMnO_3$ crystal on the laser excitation power (a) in the one-phonon spectral range, (b) in the spectral range from 520 to 2600 cm^{-1}, and (c) in the spectral range from 2000 to 6000 cm^{-1}. The local actual temperatures under the different laser excitation power, estimated from the width of the A_g phonon at 500 cm^{-1}: 10% $\sim$300 K, 25% $\sim$400 K, 50% $\sim$600 K, 100% $\sim$700 K. The dash-dotted lines indicate the PDOS main peak position periodically repeated in the multi-phonon range. The red and blue bars on the top scale denote the estimated energies of the **E** and **A** symmetry quantum rotor orbital excitations in the dynamic limit, respectively.

associated with the quantum rotor orbital excitations in the dynamic limit for the j values 17/2, 19/2, 23/2, and 27/2, respectively. Also, the additional features observed at low energies at $\sim$253 and $\sim$464 cm^{-1} could be associated with the quantum rotor orbital excitations in the dynamic limit for the j values 7/2 and 9/2, correspondingly. We would like to note that the qualitative agreement with the quantum rotor peak energies and the evident features in the Raman scattering spectra is rather good.

We would like to note that the results of the present Raman study are in agreement with our recent spectroscopic ellipsometry study of the untwinned $LaMnO_3$ crystal. There we show that the quantum rotor orbital excitations arise above the pronounced low-energy optical band located at 2 eV. In accordance with our predictions, the orbital excitations for the j values 17/2 and 19/2 appear as a doublet at 2.28 eV, the orbital excitations for the j values 23/2 and 25/2 appear as a doublet at 2.41 eV, and the orbital excitations for the j values 29/2 and 31/2 will appear as a doublet at 2.74 eV in the **a**-axis room-temperature spectra. Here the qualitative agrement with the peak energies observed in the **a**-axis spectra at 2.29, 2.41, and 2.66 eV is surprisingly good. The quantum rotor orbital excitations observed above the high-spin $d^4d^4 \rightarrow d^3d^5$ electronic transition at 2 eV can be related to the upper sheet of the "Mexican hat" adiabatic potential-energy surface [10].

From the results of the present Raman study and our earlier optical studies [9, 10] we can conclude that $LaMnO_3$ system can have low- and high- temperature dynamic limit. The high-temperature limit of the dynamic JT effect in $LaMnO_3$ occurs close to the orbital ordering temperature $T_{OO} \simeq 780$ K, where the energetic barriers in the "Mexican hat" potential profile become thermally accessible. This is illustrated by the present Raman scattering study. As a result, apart rom the anomalously strong, periodically repeated PDOS feature [9], we were able to identify additional weak features under high laser excitation power, which can be associated with the quantum rotor orbital excitations. The found behavior can be referred to the lower sheet of the "Mexican hat" adiabatic potential-energy surface, specifying the ground state properties in the high-temperature dynamic limit. However, the low-temperature dynamic limit of the JT effect in $LaMnO_3$ can also occur. The dynamic behaviour at temperatures well below the orbital ordering temperature T_{OO} was reported recently for another model material for

a cooperative JT effect, $KCuF_3$ [20]. We argue that superexchange interactions between the Mn^{3+} ions may drive the system to the dynamic-like behaviour. The magnetic interactions in magnetic oxides, and, in particular, in the $LaMnO_3$ system, are successfully described in the framework of Kugel-Khomskii model [7, 12, 21, 22, 23]. In our comprehensive spectroscopic ellipsometry study of the untwinned $LaMnO_3$ crystal, we showed that the **a**-axis kinetic energy of the e_g electrons, associated with the high-spin $d^4d^4 \rightarrow d^3d^5$ electronic transition between neighbouring Mn^{3+} ions at 2 eV, increases by about 55 meV below the Néel temperature $T_N \simeq 140$ K [12, 24]. This energy is comparable with the orbital ordering temperature of $LaMnO_3$, $T_{OO} \simeq 780$ K $= 65$ meV. Therefore, the superexchange interaction may be crucial in driving the e_g electrons into the regime of the dynamic JT effect, with affordable barriers for the tunneling between the potential energy minima. Here, one should take into account the anisotropy of the superexchange interactions in $LaMnO_3$, which results in the ferromagnetic ordering in the **ab** plane and antiferromagnetic ordering along the **c** axis. The low-temperature dynamic behaviour can be driven by ferromagnetic correlations in the **ab** plane. By contrast, the increased antiferromagnetic correlations along the **c** axis can lead to the dynamic-to-static transition at low temperature [10].

Finally, we note that the low- and high-temperature behaviour of the $LaMnO_3$ system indicates the dynamic regime of the JT effect, which can be described in the framework of the O'Brien's diagram (see Fig. 1(b)) [2]. Further experiments are needed to investigate quantum rotor orbital excitations in the JT compounds with JT ions such as Mn^{3+} or Cu^{2+} ions. The discovered orbital excitations of quantum rotors may play an important role in many unusual properties observed in these compounds upon doping, such as high-temperature superconductivity and colossal magnetoresistance.

Acknowledgments

The authors acknowledge fruitful discussions with V Hizhnyakov. We thank A Balbashov for growing the crystals. We also thank A Kulakov for detwinning the crystal, J Strempfer, I Zegkinoglou, and M Schulz for characterization of the $LaMnO_3$ sample. This work was supported by the Russian Foundation for Basic Research, projects 16-02-00304 and 17-02-00323.

References

[1] Jahn H A and Teller E 1937 *Proc. R. Soc. London* A **161** 220
[2] O'Brien M C M 1964 *Proc. Roy. Soc.* A **281** 323
[3] Bersuker I B 2006 *The Jahn-Teller Effect* (New York, Melbourne, Cape Town, Singapore, Sao Paulo: Cambridge Univ. Press).
[4] García-Fernández P, Bersuker I B, Aramburu J A, Barriuso M T and Moreno M 2005 *Phys. Rev.* B **71** 184117
[5] Kaplan M D and Vekhter B G 1995 *Cooperative Phenomena in Jahn-Teller Crystals* (New York: Plenum Press)
[6] Bersuker I B, Vekhter B G and Ogurtsov I I 1975 *Sov. Phys. Usp.* **18** 569
[7] Kugel K I and Khomskii D I 1973 *Sov. Phys. JETP* **37** 725
[8] Rodríguez-Carvajal J, Hennion M, Moussa F, Moudden A H, Pinsard L and Revcolevschi A 1998 *Phys. Rev.* B **57** R3189
[9] Kovaleva N N, Kusmartseva O E, Kugel K I, Maksimov A A, Nuzhnyy D, Balbashov A M, Demikhov E I, Dejneka A, Trepakov V A, Kusmartsev F V and Stoneham A M 2013 *J. Phys.: Condens. Matter* **25** 155602
[10] Kovaleva N N, Kugel K I, Potucek Z, Kusmartseva O E, Goryachev N S, Bryknar Z, Demikhov E I, Trepakov V A, Dejneka A, Kusmartsev F V and Stoneham A M 2016 *JETP* **122** 890
[11] Balbashov A M, Karabashev S G, Mukovsky Ya M and Zverkov S A 1996 *J. Cryst. Growth* **167** 365
[12] Kovaleva N N, Oleś Andrzej M, Balbashov A M, Maljuk A, Argyriou D N, Khaliullin G and Keimer B 2010 *Phys. Rev.* B **81** 235130
[13] Smirnova I S 1999 *Physica* B **262** 247
[14] Iliev M N, Abrashev M V, Lee H-G, Popov V N, Sun Y Y, Thomsen C, Meng R L and Chu C W 1998 *Phys. Rev.* B **57** 2872

[15] Kovaleva N N, Boris A V, Capogna L, Gavartin J L, Popovich P, Yordanov P, Maljuk A, Stoneham A M and B. Keimer 2008 *Phys. Rev.* B **79** 045114
[16] Saitoh E, Okamoto S, Takahashi K T, Tobe K, Yamamoto K, Kimura T, Ishihara S, Maekawa S and Tokura Y 2001 *Nature* **41** 180
[17] Laverdrière J, Jandl S, Mukhin A A and Ivanov V Yu 2006 *Eur. Phys. J.* B **54** 67
[18] Iliev M N, Hadjiev V G, Litvinchuk A P, Yen F, Wang Y-Q, Sun Y Y, Jandl S, Laverdière J, Popov V N and Gospodinov M M 2007 *Phys. Rev.* B **75** 064303
[19] Iliev M N, Abrashev M V, Popov V N and Hadjiev V G 2003 *Phys. Rev.* B **67** 212301
[20] Deisenhofer J, Leonov I, Eremin M V, Kant Ch, Ghigna P, Mayr F, Iglamov V V, Anisimov V I and van der Marel D 2008 *Phys. Rev. Lett.* **101** 157406
[21] Kugel K I and Khomskii D I 1982 *Sov. Phys. Uspekhi* 1982 **25** 231 [1982 *Usp. Fiz. Nauk* **136** 621]
[22] Oleś Andrzej M, Khaliullin G, Horsch P and Feiner L F 2005 *Phys. Rev.* B **72** 214431
[23] Kovaleva N N, Boris A V, Yordanov P, Maljuk A, Brücher E, Strempfer J, Konuma M, Zegkinoglou I, Bernhard C, Stoneham A M and Keimer B 2007 *Phys. Rev.* B **76** 155125
[24] Kovaleva N N, Boris A V, Bernhard C, Kulakov A, Pimenov A, Balbashov A M, Khaliullin G and Keimer B 2004 *Phys. Rev. Lett.* **93** 147204